Liquid Crystals
Publication details, including instructions for authors and subscription information:
http://www.informaworld.com/smpp/title~content=t713926090

Mononuclear and binuclear complexes of salicylidene Schiff bases: synthesis and mesogenic properties

Nandiraju V. S. Rao[a]; Trirup D. Choudhury[a]; Manoj K. Paul[a]; Tuluri Francis[b]
[a] Chemistry Department, Assam University, Silchar, Assam, India [b] Physics Department, Jackson State University, Jackson, MS, USA

To cite this Article Rao, Nandiraju V. S. , Choudhury, Trirup D. , Paul, Manoj K. and Francis, Tuluri(2009) 'Mononuclear and binuclear complexes of salicylidene Schiff bases: synthesis and mesogenic properties', Liquid Crystals, 36: 4, 409 — 423
To link to this Article: DOI: 10.1080/02678290902926892
URL: http://dx.doi.org/10.1080/02678290902926892

Liquid Crystals,
Vol. 36, No. 4, April 2009, 409–423

Taylor & Francis
Taylor & Francis Group

Mononuclear and binuclear complexes of salicylidene Schiff bases: synthesis and mesogenic properties

Nandiraju V.S. Rao[a]*, Trirup D. Choudhury[a], Manoj K. Paul[a] and Tuluri Francis[b]

[a]*Chemistry Department, Assam University, Silchar – 788 011, Assam, India;* [b]*Physics Department, Jackson State University, Jackson, MS 39217, USA*

(Received 30 December 2009; final form 26 March 2009)

The synthesis of new mononuclear and binuclear copper complexes derived from Schiff bases, namely N(4-n-alkyloxysalicylidene)-4′-n-alkylanilines is carried out and their structure and liquid crystalline properties have been investigated. The ligands exhibit rich polymesomorphism; mononuclear complexes exhibit smectic A, smectic C and smectic E phases, while the binuclear complexes mostly exhibit viscous smectic A phase. The isotropic–liquid crystalline transition temperatures of the binuclear complexes in general are found to be lower than their corresponding mononuclear homologues. It was found that the mononuclear complexes exhibit sharp liquid crystalline–isotropic transition temperatures while the binuclear complexes melts over a temperature range. The liquid crystalline phases were characterised by differential scanning calorimetry (DSC) analysis and optical polarised microscopy. X-ray diffraction studies revealed that the intermolecular distance in binuclear complexes is larger than in the mononuclear complexes.

Keywords: liquid crystals; mononuclear and binuclear copper complexes; synthesis; enthalpy; entropy; optical properties; X-ray diffraction

1. Introduction

Materials exhibiting different functional properties can be derived by a combination of organic moieties with soft material properties and metal compounds possessing inherent rich electromagnetic characteristics. During the last three decades the metallomesogens (metal-containing liquid crystalline molecules) of d- and f-block metals have attracted the attention of several research groups (*1–10*) because of their unusual geometries and novel properties such as colour, fluidity, large birefringence, polarisability, paramagnetism etc., in addition to functional properties such as spin cross-over (*11*), ferroelectricity (*12*), photorefractivity (*13*), non-linear optical characteristics (*14*), large magnetic anisotropy (*15*) and luminescent mesophases (*16*). In most of these materials extended salicylaldimine is utilised for complexation to yield mononuclear complexes with expected molecular properties. However, the introduction of further metal centres to synthesise binuclear compounds leading to the realisation of bimetallic mesogens with novel properties, which can exhibit properties such as mixed oxidation states and/or ferro/paramagnetism, is a challenging task for chemists because these properties in turn reflect the electrical and magnetic characteristics (*17–33*). The incorporation of properties such as ferromagnetic coupling and mixed oxidation states is a significant step towards producing liquid crystals with extended magnetic interactions and high electrical conductivity.

Among the reported bimetallic mesogens, the majority are diamagnetic (*17–25*) and only very few are paramagnetic (*26–33*). Although a number of binuclear complexes exhibiting liquid crystalline behaviour are known, the majority of them are limited to ortho- or cyclopalladated compounds, dicopper β-diketonate and β-enaminoketonate complexes exhibiting columnar mesomorphism. Many binuclear palladium (II) complexes possessing crown ether derivatised imines (*23, 24*), exhibiting mesomorphic behaviour are well known. Recently Paschke *et al.* (*34*) reported some mono and binuclear copper complexes co-ordinated to two ligands of extended salicylaldimines exhibiting calamitic phases. Barbera *et al.* (*35*) reported binuclear copper (II) and oxovanadium (IV) complexes of a single ligand derived from mono-, di-, or tridecyloxy-4-benzoyloxysalicylidene-3,3′-diaminobenzidine exhibiting smectic/columnar mesomorphism depending upon the number of terminal chains, while the respective ligands also exhibited a similar trend. The molecular structures of the reported examples of binuclear complexes (*26–35*) are shown in Scheme 1. The structure–property relationship has been well studied in N-(4-n-alkyloxysalicylidene)-4-n-alkylanilines and their mononuclear copper (II) complexes. The ligands exhibit rich but complex mesomorphism and hence attracted considerable attention with regard to their mesomorphism and properties. Efforts to co-ordinate copper (II) salts with the

*Corresponding author. Email: drnvsrao@gmail.com

ISSN 0267-8292 print/ISSN 1366-5855 online

DOI: 10.1080/02678290902926892
http://www.informaworld.com

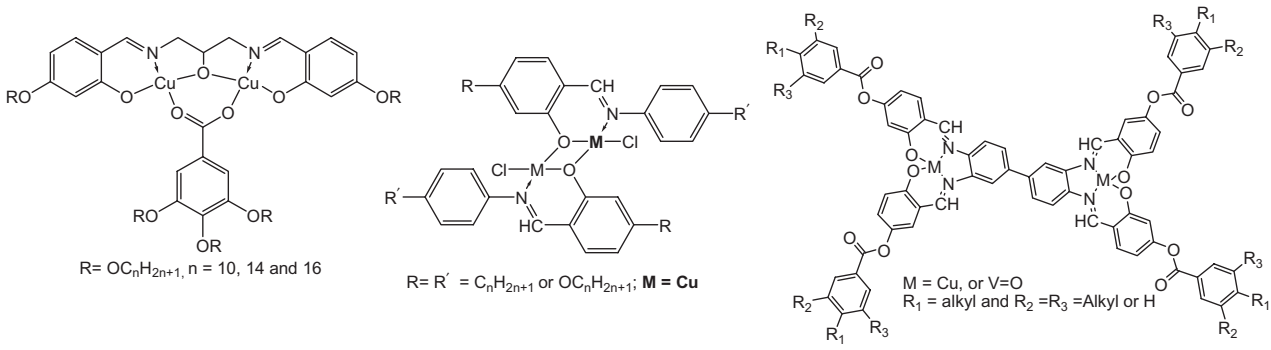

Scheme 1. Binuclear complexes.

salicylidene-based ligands to realise the binuclear copper (II) complexes are comparatively difficult in comparison to binuclear palladium (II) complexes, and hence any attempt to synthesise stable binuclear copper(II) complexes possessing new geometries and structures and exhibiting liquid crystal behaviour (*28b, 28c, 36–41*) presents an experimental challenge. In the present report we describe the synthesis and mesogenic properties of mono and binuclear paramagnetic complexes containing copper(II) co-ordinated to N-(4-n-alkyloxysalicylidene)-4′-n-alkylanilines.

2. Results and discussion

2.1 Synthesis and characterisation

The synthetic procedures for ligands N-[(4-n-alkyloxysalicylaldimine)-4′-n-alkylaniline] (hereafter abbreviated as ***4-n-m,*** where n and m indicates the number of carbon atoms in alkyl chains) as well as mononuclear copper (II) (***5-n-m***) and binuclear copper (II) complexes (***6-n-m***) are presented in Scheme 2. The Schiff bases, **4,** were synthesised by condensation of the appropriate aldehyde, **2,** with the corresponding aniline, **3,** following the literature procedures with minor modifications and were identified by ^{1}H NMR and elemental analysis (Table 1).

The mononuclear copper (II) complexes, ***5-n-m,*** were prepared by the reaction of appropriate salicylaldimine, **4,** with copper (II) acetate monohydrate in warm ethanol and recrystallised from methanol/CH_2Cl_2; the complexes were isolated as brown or green-brown solids in good yields. The formation of binuclear copper complexes, ***6-n-m,*** by the reaction of appropriate bis-N-[(4-n-alkyloxysalicylaldimine)-4′-n-alkylaniline]copper(II) complexes, **5,** with cupric chloride as shown in Scheme 2, although reflected by an immediate change in colour of the solution, was complete only after few days and in some cases a few weeks to yield as green solids. The ionisation of $CuCl_2$ salt followed by the co-ordinating ability of solvent molecules with copper (II) in solution and then reacting with mononuclear bis-N-[(4-n-

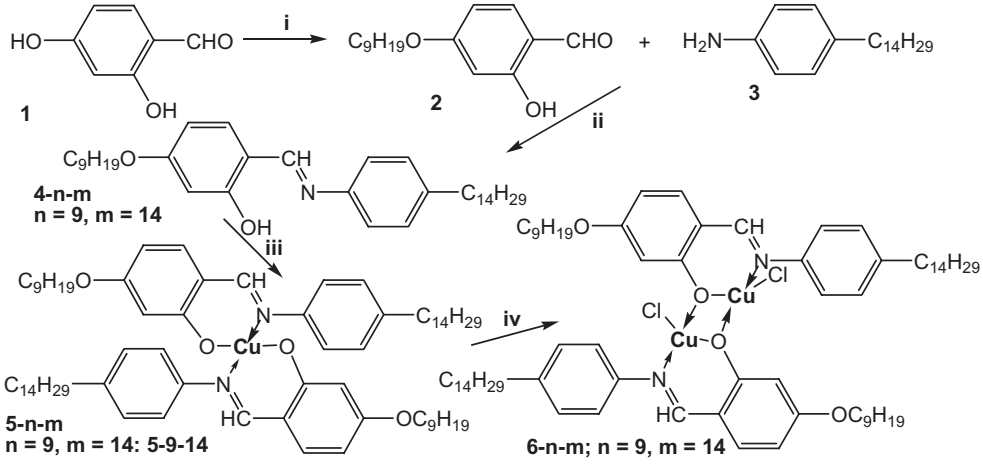

Scheme 2. **i.** $C_9H_{19}Br$, $KHCO_3$, KI, dry acetone Δ, 40h, **ii**. glacial AcOH, absolute EtOH, Δ, 4 h, **iii.** $Cu(CH_3COO)_2.H_2O$, Ethanol, Δ, 1 h, **iv.** Ethanol, $CHCl_3$, $CuCl_2$, Δ, 2 h.

Table 1. C H N analysis (figures inside the bracket are theoretical values).

	Compound code	%C percentage of Carbon	%H percentage of Hydrogen	%N percentage of Nitrogen
1.	**4-6-14**	79.83 (80.27)	10.38 (10.41)	2.48 (2.84)
2.	**5-6-14**	75.13 (75.56)	9.55 (9.61)	2.51 (2.67)
3.	**6-6-14**	66.11 (66.98)	8.43 (8.52)	2.45 (2.37)
4.	**4-9-14**	80.57 (80.69)	10.58 (10.72)	2.48 (2.61)
5.	**5-9-14**	75.91 (76.31)	9.90 (9.96)	2.88 (2.47)
6.	**6-9-14**	68.99 (68.22)	9.01 (8.91)	2.09 (2.21)
7.	**4-10-14**	80.95 (81.46)	11.22 (11.29)	2.12 (2.21)
8.	**5-10-14**	77.27 (77.69)	10.49 (10.61)	2.01 (2.11)
9.	**6-10-14**	70.33 (70.55)	9.52 (9.64)	1.81 (1.91)
10.	**4-18-14**	81.12 (81.63)	11.54 (11.42)	2.01 (2.12)
11.	**5-18-14**	77.72 (78.01)	10.54 (10.77)	2.11 (2.02)
12.	**6-18-14**	70.98 (71.11)	9.77 (9.81)	1.77 (1.84)
13.	**4-6-10**	79.27 (79.59)	9.74 (9.90)	3.09 (3.20)
14.	**5-6-10**	73.98 (74.36)	9.00 (9.04)	2.77 (2.99)
15.	**6-6-10**	64.87 (65.03)	7.76 (7.90)	2.37 (2.61)
16.	**4-12-O10**	77.95 (78.16)	10.19 (10.31)	2.47 (2.60)
17.	**5-12-O10**	73.29 (73.93)	9.34 (9.57)	2.10 (2.46)
18.	**6-12-O10**	65.98 (66.12)	8.48 (8.56)	2.01 (2.26)

alkyloxysalicylaldimine)-4′-n-alkylaniline]copper(II) complex is assumed to be the possible mechanism to yield these binuclear complexes. In view of the large time scale associated with the formation of binuclear complex it is realistic to believe that the rate-determining step is to be the co-ordination of the chloride with copper (II), shown in Scheme 3, and is in agreement with the reported results (*34*). Some of the synthesised compounds were characterised by elemental analyses, Fourier transform infrared (FT-IR) and UV–visible spectroscopy. Elemental analyses of ligands and complexes are consistent with the proposed structures, confirming the mononuclear and binuclear composition of the complexes. Detailed synthetic procedures and characterisation by the spectroscopic methods are presented in electronic supplementary information.

2.2 UV–visible spectra

The UV–visible spectra recorded in chloroform (Figure 1) for the ligand, mononuclear and binuclear complexes are found to be different but show consistent changes in the charge-transfer region. In general, distinct changes in low-energy bands with an approximate increase of 20–30 nm from ligand **4-n-m** to mononuclear complex **5-n-m (**of around 21 nm for the lower homologues and 30 nm for higher homologues) while a similar decrease in optical absorption for mononuclear complex **5-n-m** to binuclear complex **6-n-m** (Table 2, e.g., 364.0–342.0 nm from mononuclear **5-5-14** to binuclear **6-5-14**; 376–346 nm from **5-9-14** to binuclear **6-9-14** complexes) is also observed. There is a significant red shift (bathochromic) upon mononuclear complexation which was reversed (blue shifted) with the introduction of a second metal ion. The reasons for such reversal of optical transitions are unknown at present and further studies are in progress to identify plausible reasons. One possible reason for the observed close optical transitions in binuclear complexes and those of the ligands may be that the electron with drawing chloro moiety on the metal atom may be compensating the charge donation from the aromatic imine ligand to the metal. The absorption spectrum of ligand **4-9-14** consists of three intense bands (ε = 47,000–96,000 l mol^{-1} cm^{-1}) in the region between 240 and 350 nm. Upon complexation with Cu (II) **5-9-14,** the two intense shorter wavelength features mainly associated with intraligand π–π* transitions shifted to higher wavelength bands (~15 nm), while the strong longer wavelength band possessing similar band shape is red-shifted (~34 nm). The spectrum of binuclear complex **6-9-14** is dominated by three intense bands in the region of 240 and 350 nm as observed in the free ligand spectrum. The broad transition of mononuclear complex **5-9-14** exhibits a very weak hypsochromic (blue) solvatochromic shift, with representative λ_{max} nm (solvent) of 372 (hexane), 378 (benzene), 376 (chloroform), 373

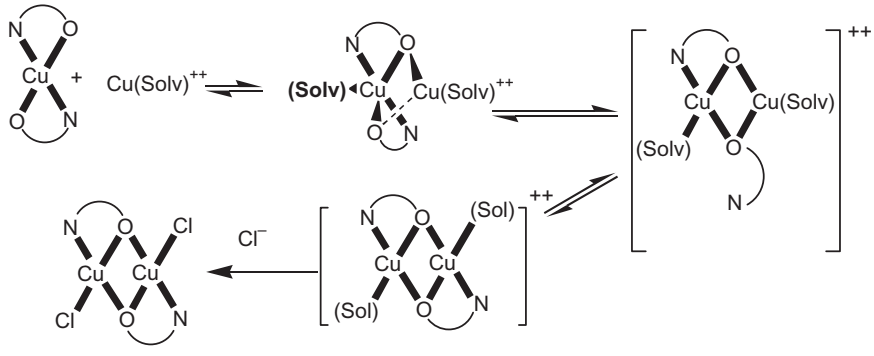

Scheme 3. Proposed mechanism for the formation of binuclear copper (II) complex.

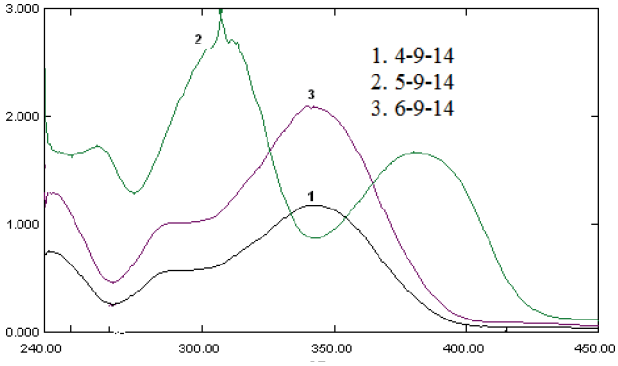

Figure 1. Optical absorption spectra of ligand ***4-9-14***, complexes ***5-9-14*** and ***6-9-14*** in chloroform solution.

Table 2. Optical absorption maxima of the compounds studied in chloroform (λ_{max}, nm).

Compound	λ_{max}	λ_{max}
4-5-14	314 (2.8)	291 (1.45)
5-5-14	364 (2.41)	309 (3.65)
6-5-14	342 (2.39)	284.8 (1.6)
4-6-14	341 (1.27)	287.4 (0.61)
5-6-14	364.8 (1.98)	310.6 (1.34)
6-6-14	343.2 (2.26)	284.8 (1.4)
4-8-14	342 (1.94)	286.9 (0.95)
5-8-14	374.5 (1.20)	307.5 (1.94)
6-8-14	343 (2.11)	290 (1.00)
4-9-14	342.5 (0.97)	289.8 (0.47)
5-9-14	376 (1.00)	306.8 (1.61)
6-9-14	346.9 (1.07)	285.5 (0.81)
4-16-14	343 (2.31)	287 (1.12)
5-16-14	374.5 (1.15)	306.5 (1.87)
6-16-14	343 (2.09)	315.4 (2.00)

(acetone) and 366 (ethyl acetate). However the UV–visible spectra recorded in solution for binuclear complexes (Figure 1) exhibited a moderate bathochromic (red) solvatochromic shift (representative λ_{max} nm (solvent) of 344 (hexane), 343 (benzene), 346 (chloroform), 360 (acetone) and 350 (ethyl acetate)), indicating changes in electronic structure. Solvatochromism is usually indicative of changes in dipole moments ($\Delta\mu$) between the ground and excited states upon excitation in metal–salen complexes. The optical transition associated with this charge transfer band (principally π–π* in character) involves both the ligand and metal centre, essentially involving the metal d_{xz}+ O_{2p} and the C=N orbitals and is the excitation mainly responsible for the nonlinear optical activity (*42–44*).

2.3 Infrared spectra

The Schiff bases in general exhibit a stretching vibration in the infrared region 1633–1623 cm^{-1} and is assigned to the imine C=N bond. This band is shifted to a lower wave number (1606–1610 cm^{-1}) upon chelation, reflecting the involvement of azomethine N atom in the metal–nitrogen bond formation. The infrared spectra of the mononuclear and binuclear complexes **5** and **6** exhibited typical behaviour and the conversion to binuclear complexes is reflected with significant characteristic changes. The distinct change in the infrared spectrum is the shift of the bands associated with the bridging oxygens, e.g., the band near 1529 cm^{-1}, is supporting evidence to assign the phenolic C–O stretching vibration in the mononuclear complex is shifted to higher energy 1540 cm^{-1}, an increase of 11 cm^{-1}, reflecting the increased constraint introduced by the oxygen bridging, and is in agreement with reported results on binuclear complexes (*34, 45, 46*). The obtained IR and ^{1}H NMR data are found to be in good agreement with the proposed structures. ^{1}H NMR spectra of the ligands show a signal at δ = 13.4–13.8 ppm, corresponding to the proton of the OH group. The hydrogen signal of the imine group appears at 8.5 ppm for ligands.

2.4 Thermal microscopy and differential scanning calorimetric studies: mesomorphic behaviour

All of the ligands N-(4-n-akoxysalicylidene)-4′-n-alkylanines, mononuclear and binuclear copper complexes exhibit liquid crystalline behaviour and were studied by thermal analysis and polarising optical microscopy with a hot stage. The phase transition temperatures and associated thermodynamic data of enthalpies and entropies for the ligands **4-n-m,** mononuclear complexes **5-n-m** and binuclear copper complexes **6-n-m,** by differential scanning calorimetry (DSC), are summarised in Tables 3, 4 and 5, respectively. All of the ligands (**4-n-m**), the mononuclear (**5-n-m**) and binuclear copper complexes (**6-n-m**) are found to exhibit mesomorphic behaviour. Phase symbols of K, SmE, SmF, SmC, SmA and I are used to denote crystalline, smectic E, smectic F, smectic C, smectic A and isotropic liquid phases, respectively. The square brackets indicate a monotropic transition. Crystalline polymorphism was often observed for solution-crystallised virgin samples of a majority of mononuclear copper complexes in the first heating cycle, and in some cases even in subsequent heating cycles, indicating the thermodynamically stable states. Such polymorphic forms may be due to the differences in molecular structures. Liquid crystalline phase identification was based on the optical textures of the sample placed between an untreated glass plate and a cover glass, and the magnitude of the isotropisation enthalpies is consistent with the assignment of each mesophase type.

Table 3. Mesomorphic phase transition temperatures (T, °C), associated enthalpies (ΔH, kJ mol^{-1}) and entropies (ΔS, J K^{-1} mol^{-1}) of the phase transitions of N-(4-n-alkoxysalicylidene)-4′-n-alkylanilines, ***4-n-m***.

	Compound	Transition	T (°C)	ΔH (kJ mol^{-1})	ΔS (J mol^{-1} K^{-1})
1.	**4-5-14**	K–SmA	54.7	47.2	144.2
		SmA–I	88.1	5.4	14.8
		I–SmA	87.3	4.5	12.7
		SmA–K	38.6	95.6	147.1
2.	**4-6-14**	K–SmA	50.5	46.4	143.4
	K[1] 48.7 (10.1,	SmA–I	98.8	7.76	20.8
	31.5) K	I–SmA	95.9	7.59	20.6
		SmA–SmF	45.2	2.22	6.98
		SmF–K	37.6	4.47	14.4
3.	**4-7-14**	K–SmA	57.6	58.6	177.7
		SmA–I	94.8	6.27	17.0
		I–SmA	93.2	4.48	12.2
		SmA–SmF	40.2	6.23	19.9
		SmF–K	38.0	35.0	112.6
4.	**4-8-14**	K–SmC	56.9	51.3	155.4
		SmC–SmA	98.1[tm]	–	–
		SmA–I	99.2	8.76	23.5
		I–SmA	98.3	8.09	21.8
		SmA–SmC	94.2 [tm]	–	–
		SmC–SmF	46.8	2.28	7.14
		SmF–SmB	37.9	3.58	11.5
		SmB–K	35.6	30.1	97.5
5.	**4-9-14**	K–SmC	63.5	58.9	175.1
		SmC–SmA	94.1 [tm]	–-	–-
		SmA–I	97.4	8.4	22.9
		I–SmA	96.3	7.8	21.1
		SmA–SmC	94.7[tm]	–	–-
		SmC–SmF	43.0	23.1	73.3
		SmF–K	41.1	15.0	47.7
6.	**4-10-14**	K–SmF	61.6	40.0	119.6
		SmF–SmC	62.7	1.42	4.2
		SmC–I	100.2	10.6	28.4
		I–SmC	99.6	10.6	28.4
		SmC–SmF	51.0	0.86	2.6
		SmF–K	34.2	14.3	46.5
7.	**4-11-14**	K–SmF	69.0	70.2	205.4
		SmF–SmC	60.3[tm]	–	–
		SmC–I	99.6	10.8	29.2
		I–SmC	98.1	9.35	25.2
		SmC–SmF	51.8	2.76	8.50
		SmF–K	48.5	55.3	171.8
8.	**4-12-14**	K–SmA	68.9	59.8	175.1
		SmA–I	100.8	12.5	33.5
		I–SmA	99.7	12.3	32.9
		SmA–SmF	58.0	3.74	11.3
		SmF–K	55.9	45.9	139.7
9.	**4-14-14**	K–SmC	73.8	63.1	181.9
		SmC–I	95.3	4.71	12.8
		I–SmC	93.5	5.15	14.1
		SmC–K	60.2	84.9	254.8
10.	**4-16-14**	K–SmC	78.2	66.7	190.3
		SmC–I	98.4	13.0	35.0
		I–SmC	97.5	11.2	30.3
		SmC–SmF	70.0	4.41	11.2
		SmF–SmG	57.2	21.3	64.7
		SmG–K	56.1	4.13	12.5
11.	**4-18-14**	K–SmC	80.9	66.8	190.5
		SmC–I	94.1	7.42	20.2
		I–SmC	93.3	7.30	19.9
		SmC-SmF	72.5	6.79	19.6
		SmF–K	54.4	47.9	146.5
12.	**4-10-O12**	K–SmF	79.5	57.1	162.1
		SmF–SmC	111.6[tm]	–	–
		SmC–I	124.0	7.52	18.9
		I–SmC	122.5	5.51	13.9
		SmC–SmF	101.4[tm]	–	–
		SmF–K	68.4	38.0	111.4

2.4.1 *Mesomorphic properties of ligands **4-n-m***

On cooling from the isotropic phase the mesophase is reflected in the form of batonnets which further coalesced to yield a focal conic fan texture characterising the phase as SmA phase in lower homologues, while the SmC phase is characterised by either a Schlieren or broken focal conic fan texture. In the same sample extinct regions were also observed, indicating homeotropic alignment of the molecules, which confirm the easy identification of SmA phase. On further cooling of SmA or SmC phase, the formation of SmF phase is inferred by the growth of either broken focal conic fan texture or Schlieren mosaic texture. Similarly, the cooling of SmA or SmC phase in the formation of SmE phase is inferred by a characteristic texture with the growth of concentric arcs within the original focal conic fan texture, or by an appearance of a scale-like mosaic texture when cooled from a homeotropic SmA phase or Schlieren texture of SmC phase. The ligands with shortest alkyloxy chain exhibited only SmA phase, while the higher homologues with increasing chain length exhibited AF, ACF, ACFB, CF, CFB

Table 4. Mesomorphic phase transition temperatures T (°C), associated enthalpies (ΔH, kJ mol^{-1}) and entropies (ΔS, J K^{-1} mol^{-1}) of the phase transitions of copper (II) complexes of N-(4-n-alkoxysalicylidene)-4′-n-alkylanilines, ***5-n-m***.

	Compound	Transition	T (°C)	ΔH (kJ mol^{-1})	ΔS (J mol^{-1} K^{-1})
13.	**5-5-14:**	K–SmE	85.2	37.3	104.3
	K^1 72.7	SmE–	106.8	10.2	26.9
	(11.9, 34.4)	SmA			
	K^2	SmA–I	136.0	8.3	20.5
	K^2 76.7	I–SmA	134.8	7.6	18.6
	(1.1, 3.2) K	SmA–	83.2	9.5	26.7
		SmE			
		SmE–K	53.2	8.3	25.7
14.	**5-6-14**	K–SmE	92.6	42.7	116.7
		SmE–	115.9	18.9	48.7
		SmA			
		SmA–I	133.9	12.5	30.8
		I–SmA	133.2	11.7	29.0
		SmA–	92.4	6.9	18.9
		SmE			
		SmE–K	55.2^{tm}	–	–
15.	**5-8-14**	K–SmE	93.9	44.4	121.0
		SmE–	116.1	19.5	50.3
		SmC			
		SmC–	126.1^{tm}	–	–
		SmA			
		SmA–I	134.4	12.2	30.0
		I–SmA	133.2	12.6	31.1
		SmA–	117.1 ^{tm}	–	–
		SmC			
		SmC–	91.6	7.4	20.5
		SmE			
		SmE–K	60.6^{tm}		
16	**5-9-14**	K–SmE	100.5	40.7	108.9
		SmE–	115.6	23.9	61.5
		SmF			
		SmF–	123.4	0.3	0.7
		SmC			
		SmC–	130.4	–	–
		SmA			
		SmA–I	132.1	11.3	28.0
		I–SmA	131.1	11.3	28.0
		SmA–	128.8	–	–
		SmC			
		SmC–	122.8	0.3	0.7
		SmF			
		SmF–	92.7	4.5	13.1
		SmE			
		SmE–K	59.9	2.00	6.0
17.	**5-10-14**	K–SmE	98.1 [97.9]	16.1	43.4
	K^{1}73.9 (4.84)		(*15*)	[37.3]	
	[72.0, (10.7)]	SmE–	117.9	26.4	67.5
		SmC			
		SmC–	124.0	0.37	0.95
		SmA	[104.5]	[12.1]	
		SmA–I	131.0	12.5	31.0
			[123.8]	[12.2]	
		I–SmA	129.7	11.8	29.3
		SmA–	122.7	0.22	0.55
		SmC			
		SmC–	91.7	9.8	26.9
		SmE			
		SmE–K	62.4	1.32	3.75
18.	**5-11-14**	K–SmE	108.1	52.8	138.7
		SmE–	117.5	25.9	66.4
		SmF			
		SmF–	125.5	0.51	1.28
		SmA			
		SmA–I	129.6	17.4	43.3
		I–SmA	128.7	15.7	38.9
		SmA–	125.1	0.45	1.15
		SmF			
		SmF–	94.1	30.9	84.3
		SmE			
		SmE–K	65.7	6.87	18.1
19.	**5-14-14**	K–SmE	92.2	6.89	18.8
		SmE–	115.9	85.1	218.9
		SmF			
		SmF–	125.4 ^{tm}	–	–
		SmA			
		SmA–I	125.6	14.2	35.6
		I–SmA	124.3	14.6	36.8
		SmA–	124.1 ^{tm}	–	–
		SmF			
		SmF–	99.3	18.7	50.2
		SmE			
		SmE–K	58.8^{tm}	–	–
20.	**5-16-14**	K–SmC	113.6	114.8	297.1
	K^1 103.2	SmC–I	121.4	17.2	43.6
	(15.1, 40.1) K	I–SmC	120.4	16.3	41.5
		SmC–	100.4	24.8	66.6
		SmE			
		SmE–K	54.0^{tm}	–	–
21.	**5-18-14**	K–SmE	66.8	4.82	14.2
		SmE–	79.7	58.9	167.1
		SmC			
		SmC–I	94.7	9.66	26.2
		I–SmC	92.1	7.92	21.7
		SmC–	76.1	10.6	30.4
		SmE			
		SmE–K	44.6	9.29	29.2
22.	**5-10-O12**	K–SmC	132.2[134]	45.5[44.8]	112.4
	K^1 104.3		(*5*)		
	(33.2, 88.2) K	SmC–	147.8[147]	0.6 [–]	1.6
		SmA			
		SmA–I	149.5[151]	10.8	25.6
				[10.9]	
		I–SmA	148.2	12.5	29.8
		SmA–	146.0^{tm}	–	–
		SmC			
		SmC–K	101.7	32.5	86.9

Table 5. Mesomorphic phase transition temperatures T (°C), associated enthalpies (ΔH, kJ mol^{-1}) and entropies (ΔS, J K^{-1} mol^{-1}) of the phase transitions of binuclear copper (II) complexes of N-(4-n-alkoxysalicylidene)-4′-n-alkylanilines, ***6-n-m***.

	Compound	Transition	T (°C)	ΔH (kJ mol^{-1})	ΔS (J mol^{-1} K^{-1})
23.	**6-5-14**	K–SmA	90.6	5.3	14.7
		SmA–I	116.8	1.6	4.1
		I–SmA	110.8	1.3	3.38
		SmA–K	55.0	4.9	14.9
24.	**6-6-14**	K–SmA	68.2	59.3	173.7
		SmA–I	106.1	3.4	8.96
		I–SmA	103.2	1.2	3.18
		SmA–K	35.0[1]	–	–
25.	**6-8-14**	K–SmA	93.9	17.3	47.4
		SmA–I	108.8	7.8	20.6
		I–SmA	108.4	7.9	20.7
		SmA–K	34.0[1]	–	–
26.	**6-9-14**	K–SmE	52.1	10.3	31.9
		SmE–SmA	92.0	22.1	60.6
		SmA–I	106.1	1.5	3.9
		I–SmA	104.6	5.0	13.4
		SmA–SmE	62.1	22.3	66.7
		SmE–K	34.4[1]	–	–
27.	**6-16-14**	K–SmE	69.4	0.49	1.45
		SmE–SmC	101.4	4.26	11.3
		SmC–I	112.7	27.1	70.6
		I–SmC	112.6[1]	5.63	14.3
		SmC–SmE	97.1[1]	3.44	8.93
		SmE–K	35.6	4.49	12.1
28.	**6-18-14**	K–SmA	63.1	5.64	16.7
		SmA–I	78.4	60.1	171.4
		I–SmA	78.2	3.4	9.7
		SmA–K	36.4	1.0	3.3
29.	**6-10-O12**	K–SmE	92.8 [81.9]	51.4 [26.8]	140.6
		SmE–SmA	104.9	11.4	30.2
		SmA–I	127.7 [127.2]	13.3 [3.9]	33.2
		I–SmA	122.1	2.63	6.66
		SmA–SmE	63.1[3]		
		SmE–K	60.5	28.2[3]	84.6[2]

[1]Thermal microscopy.
[2]Glass transition.
[3]Unresolved enthalpy and entropy values of SmA–SmE and SmE–I transitions.

phase variants. The ligand **4-8-14** exhibited a phase variant ACFB and the microscopic photographs of the corresponding phases observed in the cooling cycle in an unidirectional polyimide coated 5 μm thin commercial cells (Instec Inc. U.S.A.) are shown in Figure 2(a)–(e). The phase transition temperatures exhibited by different ligands, **4-n-m,** in the cooling cycle are shown in Figure 3. The odd–even effect in the

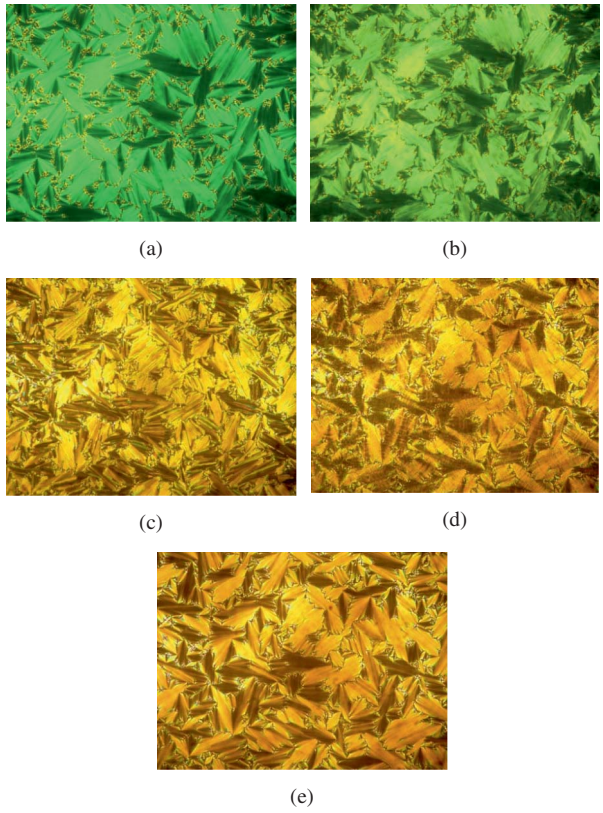

Figure 2. Textures of different smectic phases exhibited by the ligand **4-8-14**. (a) Focal fan texture exhibited by **4-8-14,** in SmA phase at 96°C in an unidirectional rubbed polyimide coated 5 μm thin cell. (b) Broken focal fan texture by **4-8-14,** at 91.2°C in SmC phase. (c) Broken focal fan texture exhibited by **4-8-14,** in SmF phase at 45.1°C. (d) Transient transition bars across the fan texture exhibited by SmF–SmB phase transition at 37.8°C. (e) Smooth focal fan texture exhibited by **4-8-14,** in SmB phase at 42°C.

homologues n = 5–12 is observed in melting as well as clearing transition temperatures. Although in some cases a pseudo-isotropic texture is observed because of long end alkyl chains, the compounds usually exhibit typical textures for the corresponding phases.

*2.4.2 Mesomorphic properties of mononuclear copper complexes **5-n-m***

The phase transition temperatures exhibited by different mononuclear complexes, **5-n-m,** in the cooling cycle are shown in Figure 4. The lower homologues of mononuclear copper (II) complexes exhibit phase variant AE while the middle homologues exhibited ACE or ACFE variants (Figure 4). The higher homologues exhibited the CE variant. The viscosity of the mesophases is normal with their fluidity, which is evident by a change in texture by shearing of the cover glasses at any temperature in the mesophase.

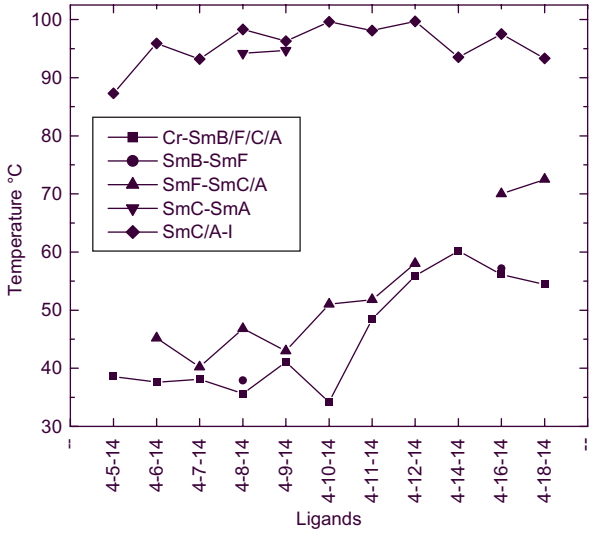

Figure 3. Phase transition temperatures of as function of chain length in ligands **4-n-m**.

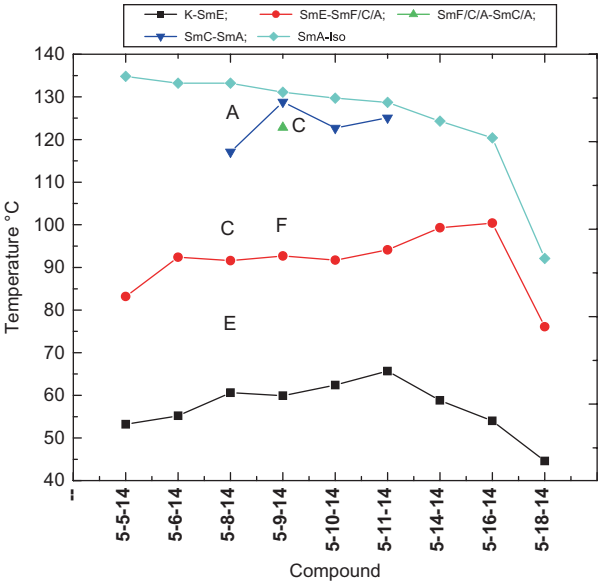

Figure 4. Phase transition temperatures of as function of chain length in mononuclear complexes, **5-n-m**.

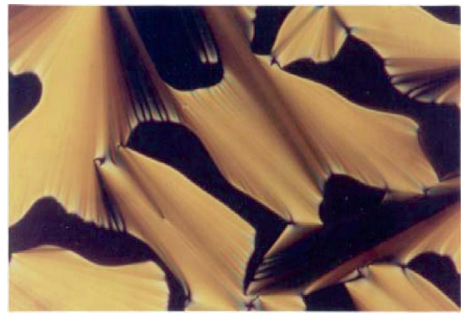

(a)

(b)

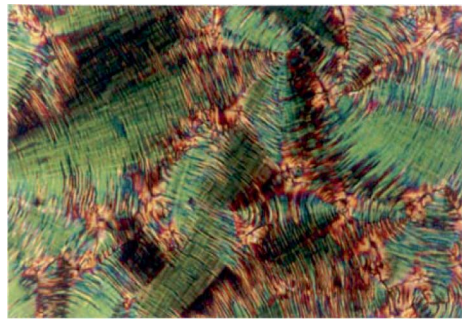

(c)

Figure 5. Textures of different smectic phases exhibited by the mononuclear complex **5-9-14**. (a) Focal conic fan texture of SmA phase exhibited by **5-9-14** at 131°C SmA. (b) Chequer board texture of SmF phase exhibited by **5-9-14** at 122.2°C. (c) Arced fan texture of SmE phase exhibited by **5-9-14** at 88°C.

Typical photographs of the textures of SmA, SmF and SmE exhibited by **5-9-14** are presented in Figure 5(a)–(c).

Some of the complexes in the present study have been reported earlier, and re-examination of freshly prepared samples to make a comparison with the reported data of the complexes revealed interesting observations. All of the compounds reported in the present work are new except **5-10-O12** (*34*) and **5-10-14** (*55*). The observed and reported transition temperatures as well as enthalpies for the compound **5-10-O12** are found to be in good agreement (K 132.2 SmC 147.8 SmA 149.5 I; reported K 134 SmA 147 SmC 151 I). However, the examination of another compound **5-10-14** (observed: Cr1 73.9 Cr2 98.1 SmE 117.9 SmC 124.0 SmA 131.0 I; reported: Cr1 72 Cr2 97.9 SmC 104.5 SmA 123.8 I, Table 3) revealed an additional liquid crystalline phase, SmE, and with a higher clearing temperature. A significant deviation in associated enthalpies and the detection of an additional phase are the new findings, while the melting

and clearing temperatures are found to be in good agreement. The SmA-SmC transition is also detected in the present work both by DSC and thermal microscopy, which was not reported earlier.

2.4.3 Mesomorphic properties of binuclear complexes ***6-n-m***

The melting and clearing phase transition temperatures in the cooling cycle for the binuclear dichlorodicopper(II) complexes of N-[(4-n-alkoxysalicylidene)-4′n-alkylanilines] **6-n-m** are illustrated in Figure 6.

The binuclear complexes exhibited mostly the phase variant A or AE. In these compounds the decrease in molecular anisotropies and a weakened or vanishing dipole contribution of the molecules due to antiparallel arrangement of dipoles in each of the molecules, and segregation of extended alkyl chains compared with those of ligands, affects the formation of tilted smectic phases and hence promote the growth of orthogonal smectic phases like SmA and SmE phases. Further, the binuclear complexes are highly viscous, evident in the transformation from isotropic to mesomorphic phase and in the paramorphotic texture in mesophase down to room temperature during slow cooling of the sample. When cooling the mesophase no transformation is observed in the microscope texture, and when frozen into the solid state a glassy mesophase is detected. The glass formation is deduced from the absence of response to shear the sample. On further cooling of the sample, conchoidal fractures appeared in the texture reflecting glassy state analogous to the glassy state in polymers. This type of phase

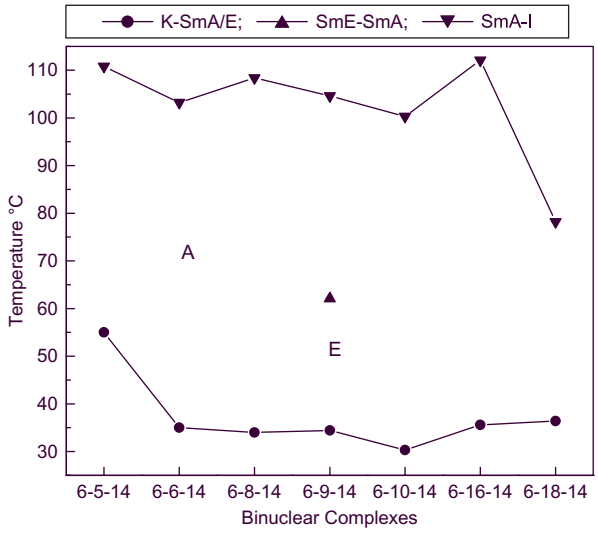

Figure 6. Phase transition temperatures of as function of chain length in binuclear complexes, **6-n-m**.

transformation is also indicated in the DSC thermogram with a broad temperature range. The difference in transition temperatures between the microscopic observation and DSC do not contradict each other because the microscopic observation is made on a thin film while DSC was carried out on a bulk sample. The majority of the binuclear complexes crystallised only partially and the enthalpy values for the crystallisation in the cooling cycle of some compounds **6-n-m** are lower than expected. The SmA phase is the commonly observed phase with few exceptions **6-9-14** (AE), **6-16-14** (AE) and **6-10-O12** (AE). However, with the increasing chain length, the higher homologues of the binuclear compounds are found to exhibit a biphase variant, namely AE, with the exception of C16 homologue (mono variant). Hence such an increase in chain may promote multiphase variants depending upon chain length variation in these dichlorodicopper(II) binuclear systems.

The textures of analogous phase variants AC or AE in the mononuclear **5** and binuclear complexes **6** exhibit an analogical appearance, with an almost comparable layer thickness in both types of complexes, in spite of differences in molecular shapes, which reflects the identical anisotropic geometry of molecular arrangement. Careful examination of the sample **6-10-O12** revealed both qualitative and quantitative deviations either in the reported thermodynamic data or phase behaviour (present work: K 92.8 SmE 104.9 SmA 127.7 I, in heating cycle; reported K 81.9 SmA 127.2 I (*34*)). We have discovered an additional liquid crystalline phase not previously established in earlier studies (*34*), crystalline smectic E phase, which is enantiotropic, i.e. observed in heating and cooling cycles.

Figure 7 illustrates the clearing temperatures of ligands, mononuclear and binuclear complexes. It is observed that the thermal stability of the mononuclear complexes is much higher than that of the ligands, and moderately higher than that of the binuclear complexes. Further, elongation of the alkyloxy chains not only affects clearing and melting temperatures but also causes a decrease in the thermal stability of mononuclear and binuclear complexes. The chemical stability of binuclear complexes **6** is also diminished compared with the mononuclear complexes **5**. Hence differences in chemical structure can account for such observations. The wider binuclear complexes, with a Cl–Cu–$(O)_2$–Cu–Cl bridge affecting the length-to-breadth ratio, weak Cl–Cu chemical bonds decreasing the chemical stability and with changes in stereo chemical structure, influence the mesophase stability of binuclear compounds. Moreover, the mononuclear or wider binuclear complexes with identical monosubstituted alkyl chains at both ends do not form a columnar phase, in agreement with the reported

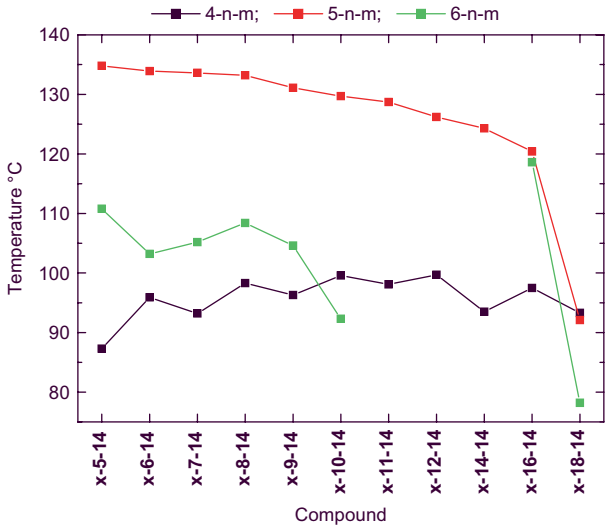

Figure 7. Mesomorphic–isotropic phase transition temperatures of ligand, **4-n-m** mononuclear complexes, **5-n-m** and bi-nuclear complexes, **6-n-m** as a function of chain length.

results on palladium dimers (*56*), while complexes with increased number of bi- or tri-substituted alkyl terminal chains exhibited columnar phases (*57, 58*). Further, the extended Schiff base tetradentate ligands possessing long alkyl chains exhibit mesomorphism, but their binuclear copper complexes did not exhibit mesomorphism though they exhibit anti-ferromagnetic exchange interaction (*59*).

2.5 X-ray studies

Examination of molecular self-organisation in the liquid crystalline phase was carried out by X-ray diffraction for representative examples of mono and binuclear copper (II) complex ***5-9-14*** and ***6-9-14***. The X-ray spectra obtained at different temperatures for mononuclear copper (II) complex ***5-9-14*** are presented in Figure 8.

The application of Bragg's law to these data gives information about the molecular arrangement in the smectic phases. The main features displayed by these spectra are the absence of the nematic phase and the presence of smectic phases. The detailed spectral analysis of the sharp and intense peak at low angle indicates a layered arrangement and a broad diffuse halo in the wide-angle region, which is characteristic of terminal hydrocarbon chains in a conformationally disordered state of smectic phases with fluidity. Further, the mononuclear complex **5-9-14** forms a

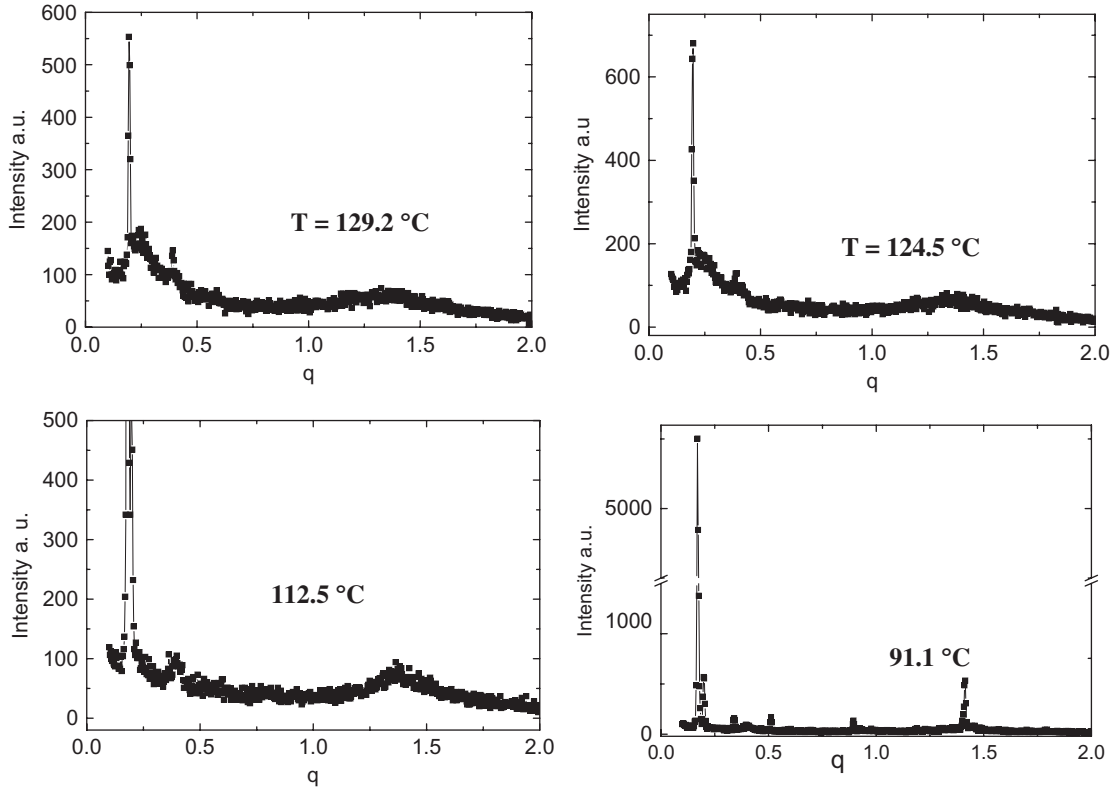

Figure 8. Typical X-ray spectra at different temperatures of mononuclear copper (II) complex **5-9-14,** at different temperatures.

sequence of monolayer-type smectic phases, with layer spacing incompatible with estimated molecular length, and with a growing degree of intra-layer molecular ordering with lowering temperature. The monolayer structure of the phases was determined from the X-ray patterns in reciprocal space recorded at different temperatures (Figure 9), which exhibited one sharp peak at $q_0 = 2\pi/d$, where $d = L\cos(\theta)$, L being the molecular length and θ the tilt angle. The variation in molecular layer thickness with temperature is illustrated in Figure 9.

The molecular length is found to be 3.22 nm in SmA phase, 3.10 in SmC phase, ~3.51 in SmF phase and increased to 3.71 nm in SmE phase for the mononuclear complex. The higher harmonics of the signal related to the layer spacing in the SmE phase were also observed. Assuming the conformation of the minimised model for compound **5-9-14,** shown in Figure 10, in which the methylene units of the end chains are in a fully extended all trans-conformation, the calculated average molecular length is 4.04 nm. However, assuming that the ends of the molecules

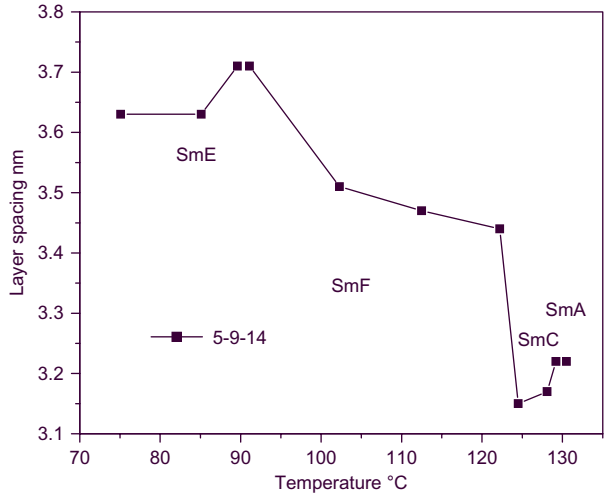

Figure 9. Temperature variation of molecular layer thickness of mononuclear copper complex **5-9-14** in different phases.

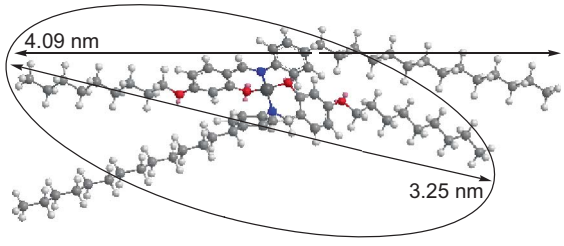

Figure 10. Molecular model of mononuclear copper (II) complex **5-9-14**.

are either folded or dispersed in the interfacial region with an approximate overlap of 0.80 nm, the calculated molecular length of 3.25 nm accounts for the experimental value of 3.22 nm in SmA phase. From the experimental layer thickness, which is found to be much smaller than the theoretical molecular length, one can envisage the possibility of either completely melted aliphatic chains or an interdigitated molecular structure. The equivalence of layer thickness and molecular length reported earlier in several calamitic molecules with free rotation of molecules is not observed in these compounds (*47*). Such a hypothesis negates the equivalence of molecular length and layer thickness here, and hence an alternative approach is needed. This envisages a completely different molecular architecture, with an anisotropic brick-like shape with free space between the two ligands separated by a metal ion in the complex, allowing the interdigitation of alkyl chains of other molecules or partial melting of aliphatic chains. This spreads out at the interface or interdigitation into adjacent layers or partial folding of extra alkyl chains situated on the same side of the molecule to effectively fill the extra space between the molecules, which can explain the observed layer spacing. Such an assumption leads to a significant reduction in effective molecular length reflecting the layer thickness because of large numbers of methylene units present in the chain. Even in earlier studies (*48, 49*) it was observed that the co-ordination of two salicylaldimine groups to a copper atom in a cisoid arrangement forces them to adopt a non-parallel arrangement which in turn gives rise to an opening of the mesogenic branches. This generates an empty space capable of accommodating end tails of hydrocarbon chains of molecules in an adjacent layer. The larger value of the intermolecular distance ~0.45 nm, compared with pure ligands, also lends support to the theory of interdigitation and spreading of end alkyl chains in the plane of the smectic layers.

Earlier studies on copper complex **5-12-4** also reported such a discrepancy between the layer thickness (3.08 nm) and molecular length (4.24 nm). The small increase in layer thickness of 0.14 nm from **5-12-4** (*12*) **to 5-9-14** (present work) cannot justify the increment of seven methylene units. The reported two-dimensional array of interdigitated molecules with a Cu–Cu correlation at 0.385 nm, as found by EXAFS measurement (*53*), supports the above observations. In liquid-like SmA and SmC phases, only one diffused signal is observed which is related to the mean intermolecular distance of ~0.45 nm for the mononuclear complex. However, the increase of the in-plane order could be observed as changes in the wide-angle region of X-ray diffraction patterns, as well as changes in the mean intermolecular distance

0.45 nm for the complex. In the hexatic smectic F phase exhibited by the mononuclear complex the peak becomes sharper, indicating a growing correlation length of the positional in-plane molecular order. At low temperature many small peaks appear in the wide-angle region and the displayed pattern resembles the patterns observed in crystalline smectic E phase which, according to international convention, is denoted as the crystal E phase (*54*).

The molecular layer thickness of binuclear copper complex **6-9-14** determined from the X-ray diffraction spectrum (Figure 11), assuming the molecular conformation shown in Figure 12, is found to be 3.50 nm, which is little larger than the mononuclear complex but is still smaller than the estimated molecular length of 4.27 nm. Hence, it is assumed that the aliphatic chains are either interdigitated or partially melted to arrange themselves like mononuclear complexes, explaining the discrepancy between the experimental layer thickness and estimated molecular length. The layer thickness in SmA and SmE phases is plotted in Figure 13. In the liquid-like but highly viscous SmA phase only one diffuse signal at wide angle is observed which is related to the mean intermolecular distance of 0.48 nm for the binuclear complex, accounting for the larger inter-molecular separation than in the mononuclear complexes (0.45 nm). Further, the intense sharp peak at 1.54 nm reflects the existence of pairs

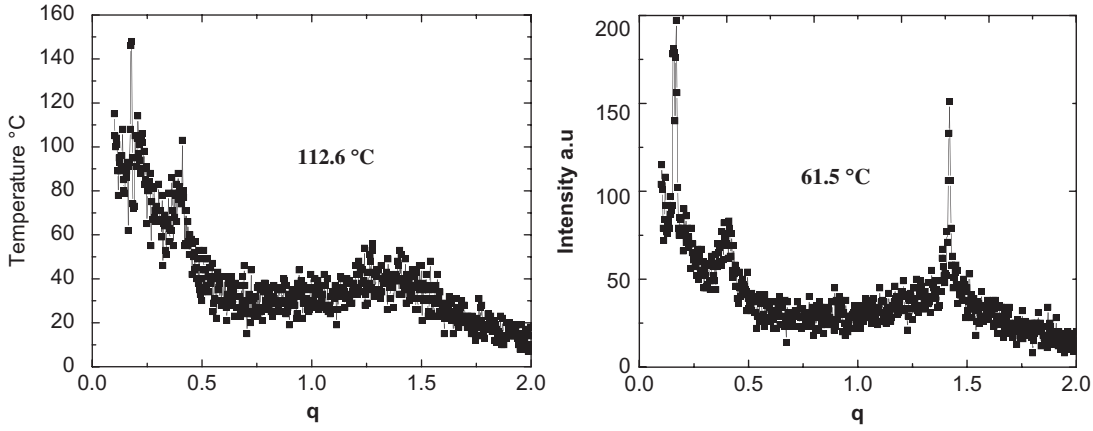

Figure 11. Typical X-ray spectra at different temperatures of binuclear copper (II) complex **6-9-14**.

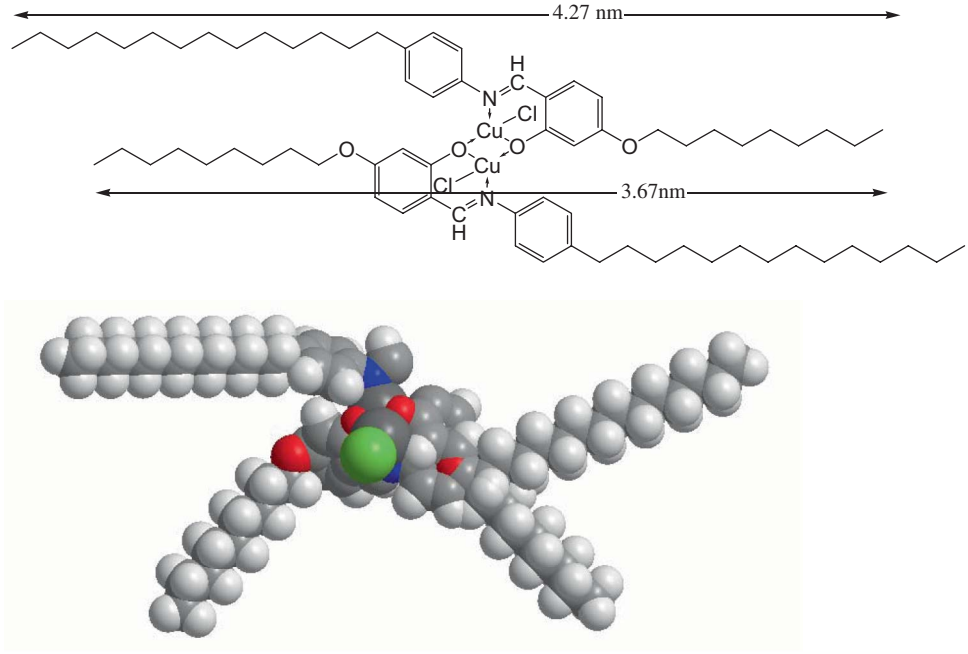

Figure 12. Molecular model of binuclear copper (II) complex **6-9-14**.

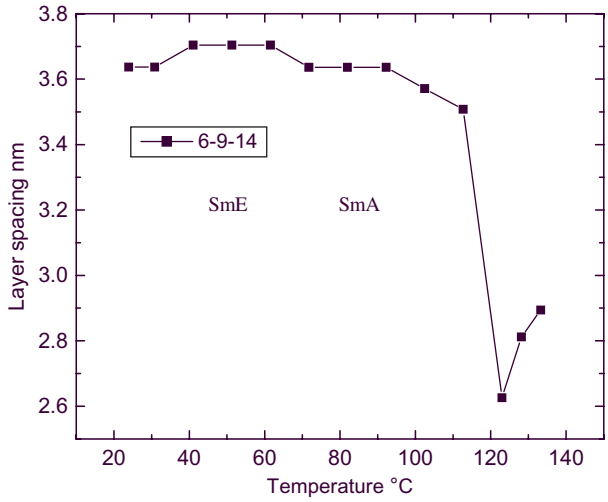

Figure 13. Temperature variation of molecular layer thickness of binuclear copper complexes **6-9-14** in different phases.

of two complexes with adjacent faces, which can account for the core length comprising of an aromatic core embedded with copper and chlorine atoms. The intense and sharp peak indicates the interferences between two Cu–Cu pairs with an extended ribbon-like molecular architecture in binuclear complexes. At low temperature many small peaks appear in the wide-angle region and the displayed pattern resembles the patterns observed in smectic phase, which accounts for the crystalline SmE phase.

3. Conclusions

The synthesis of binuclear copper (II) complexes **6** from mononuclear bis(salicylaldimine)copper(II) complexes **5** exhibiting liquid crystalline behaviour with additional phases in some cases is successful. The central core predominantly influences not only the molecular architecture in both mononuclear and binuclear complexes with tetrahedral conformation at copper (II) ion but also mesomorphic behaviour. The core length of 3.25 nm estimated from the molecular model with a tetrahedral conformation in mononuclear complexes (Figure 10) is found to be in agreement with the layer thickness (3.22 nm in SmA, 3.71 nm in SmE phase and 3.63 nm in crystalline phase). The estimated core length for the binuclear complex (Figure 12), in spite of an increased breadth-to-length ratio, is 3.68 nm, which is also in good agreement with the observed layer thickness of 3.50 nm in SmA phase, 3.70 nm in SmE phase and 3.63 nm in crystalline phase. The observed difference in molecular layer thickness in SmA phase of mononuclear and binuclear complexes can be attributed to more freedom of rotation in mononuclear complexes. Further, the rigidity of binuclear complexes is indicated by the highly viscous nature of these compounds after melting. Moreover, the flat rectangular brick-like central core of the binuclear complexes, consisting of aromatic cores augmented by additional copper(II) ion with tetrahedral stereochemistry and two chloro ligands, predominantly enhances the polarity of the core region and thereby introduces additional van der Waals and dipole interactions. The alkyl tail elongation works as a weak perturbation on the intermolecular forces necessary for the new mesophase formation, and the phase diagram represents the mesogenicity of a given molecular framework. Hence such ordered molecular structures possessing the necessary anisotropic molecular structure with enhanced microphase segregation of disordered or spread-out end alkyl chains in spite of increased breadth-to-length ratio still promoted mesomorphism. The increase in viscosity, lowering of the mesophase stability and a decrease of the melting and clearing temperatures compared with the mononuclear complexes further evidences the distortion and rigidity in molecular geometry. Some of the mononuclear complexes exhibited solid–solid phase transitions in second and third heating and cooling cycles as evidenced in DSC, but are not detected in thermal microscopy. These binuclear copper (II) compounds of N-[(4-n-alkoxysalicylidene)-4′n-alkylanilines] (N-aryl ring with 4-substituted alkyl chain) are new addition to the understanding of structure–property relationship in materials chemistry in the area of binuclear metallomesogens. A large number of compounds with different end substituents are necessary to make model compounds for different applications of new materials.

Acknowledgements

Financial assistance provided by DST, DRDO, DAE, and UGC, India is gratefully acknowledged. We thank Professor N.A. Clark and Dr C. Jones for their help in providing the experimental facility to obtain X-ray data.

References

(1) Serrano, J.L., Ed. *Metallomesogens, Synthesis, Properties and Applications*, VCH: Weinheim, 1996.
(2) (a) Giroud-Godquin, A.M. In: *Handbook of Liquid Crystals*, Demus, D.; Goodby, J.; Gray, G.W.; Spiess, H.-W.; Vill, V., Eds.; Wiley-VCH: Weinheim, Germany, 1998, Vol. IIB, pp. 901–932. (b) Giroud-Godquin, A.M.; Maitlis, P.M. *Angew. Chem. Int. Ed. Engl*. **1991**, *30*, 375–402.
(3) Espinet, P.; Esteruelas, M.A.; Oro, L.A.; Serrano, J.L.; Sola, E. *Coord. Chem. Rev*. **1992**, , *117*, 215–274.

(4) (a) Bruce, D.W. In *Inorganic Materials*, 2nd Edn., Bruce, D.W.; O'Hare, D., Eds.; Wiley: Chichester, 1996; Ch. 8. (b) Bruce, D.W.; *J. Chem. Soc. Dalton Trans*. **1993**, 2983–2989.
(5) Polishchuk, A.P.; Timofeeva, T.V. *Russ. Chem. Rev*. **1993**, *62*, 291–321.
(6) Hudson, S.A.; Maitlis, P.M. *Chem. Rev*. **1993**, *93*, 861–865.
(7) Oriol, L.; Serrano, J.L. *Adv. Mater*. **1995**, *7*, 348–369.
(8) Hoshino, N.; *Coord. Chem. Rev*. **1998**, *174*, 77–108.
(9) (a) Donnio, B.; Bruce, D.W. *Struct. Bond.*, **1999**, *95*, 193–247; (b) Donnio B.; Guillon D.; Deschenaux R.; Bruce D.W. In *Comprehensive Coordination Chemistry II: From Biology to Nanotechnology*; McCleverty, J.A.; Meyer, T.J., Eds.; Elsevier: Oxford, 2003; pp. 7, 357–627.
(10) Bruce, D.W.; Deschenaux, R.; Donnio, B.; Guillon D. In *Comprehensive Organometallic Chemistry III*; Crabtree, R.H.; Mingos, D.M.P., Eds.; Elsevier: Oxford, 2007; Vol 12. Ch.12.05, 195–293.
(11) Hayami, S.; Moriyama, R.; Shuto, A.; Maeda, Y.; Ohta, K.; Inoue, K. *Inorg. Chem*. **2007**, *46*, 7692–7694.
(12) Iglesias, R.; Marco, M.; Serrano. J.L.; Sierra, T.; Perez-Jubindo, M.A. *Chem. Mater.* **1996**, *8*, 2611–2617.
(13) Talarico, M.; Barbario, G.; Pucci, D.; Ghedini, M.; Golemme, A. *Adv. Mater*. **2003**, *15*, 1374–1377.
(14) Barbera, J.; Elduque, A,; Gimenez, R.; Lahoz, F.J.; Lopez, J.A.; Oro, L.A.; Serrano, J.L.; Villacampa, B.; Villalba, J. *Inorg. Chem*., **1999**, *38*, 3085–3092.
(15) Binnemans, K.; Galyametdinov, Y.G.; Deun, R.V.; Bruce, D.W.; Collison, S.R.; Polishchuk, A.P.; Bikchantaev, I.; Hasse, W.; Prosvirin, A.V.; Tinchurina, L.; Litvinov, I.; Gubajdullin, A.; Rakhatullin, A.; Uytterhoeven, K.; Meervelt, L.V. *J. Am. Chem. Soc*., **2000**, *122*, 4335–4344.
(16) Terazzi, E.; Suarez, S.; Torelli, S.; Nozary, H.; Imbert, D.; Mamula, O.; Rivera, J.P.; Guillet, E.; Benech, J.M.; Bernardinelli, G.; Scopelliti, R.; Donnio, B.; Guillon, D.; Bunzli, J.C.G.; Piguet, C. *Adv. Funct. Mater*. **2006**, *16*, 157–168.
(17) (a) Espinet, P.; Etxebarria, J.; Marcos, M.; Perez, J.; Remon, A.; Serrano, J.L. *Angew. Chem., Int. Ed. Engl*. **1989**, *28*, 1065–1066; (b) Espinet, P.; Lalinde, E.; Marcos, M.; Perez, J.; Serrano, J.L. *Organometallics* **1990**, *9*, 555–560.
(18) Barbera, J.; Espinet, P.; Lalinde, E.; Marcos, M.; Serrano, J.L. *Liq. Cryst*. **1987**, *2*, 833–842.
(19) Baena, M.J.; Buey, J.; Espinet, A.; Kitzerov, H.S.; Heppke, G. *Angew. Chem., Int. Ed. Engl.* **1993**, *32*, 1201–1203.
(20) Eguchia, S.; Nozaki, T.; Miyasaka, H.; Matsumoto, N.; Okawa, H.; Kohata, S.; Hosino-Miyajima, N. *J. Chem. Soc., Dalton Trans*. **1996**, 1761–1766.
(21) (a) Ghedini, M.; Pucci, D.; Munno, G.D.; Viterbo, D.; Neve, F.; Armentano, S. *Chem. Mater.* **1991**, *3*, 65–72; (b) Ghedini, M.; Longeri, M.; Bartolino, R. *Mol. Cryst. Liq. Cryst.* **1982**, *84*, 207–211; (c) Ghedini, M.; Licoccia, S.; Armentano, S.; Bartolino, R. *Mol. Cryst. Liq. Cryst.* **1984**, *108*, 269–275; (d) Ghedini, M.; Armentano, S.; Neve, F. *Inorg. Chim. Acta* **1987**, *134*, 23–24.
(22) Eran, B.B.; Singer, D.; Praefke, K. *Eur. J. Inorg. Chem*. **2001**, 111–116.
(23) Leu, Y.F.; Lai, C.K. *J. Chinese Chem. Soc*., **1997**, *44*, 89–91.
(24) Arias, J.; Bardaji, M.; Espinet, P.; *Inorg. Chem.* **2008**, *47*, 3559–3567. Arias, J.; Bardaji, M.; Espinet, P. *J. Organomet. Chem.* **2006**, *691*, 4990–4999.
(25) Diez, L.; Espinet, P.; Miguel, J.A.; Medina, M.P.R. *J. Organomet. Chem.* **2005**, *690*, 261–268.
(26) Lai C.K.; Serrete A.G.; Swager, T.W. *J. Am. Chem. Soc.* **1992**, *114*, 7948–7949.
(27) Pyzuk W.; Krowcznsky A.; Chen L.; Gorecka E.; Bickczantaev I. *Liq. Cryst*. **1995**, *19*, 675–677.
(28) (a) Lai C.K.; Chen F.G.; Ku, Ch. Y.J.; Tsai H.; Lin R.J. *J. Chem. Soc., Dalton Trans.* **1997**, 4683–4687; (b) Lai C.K.; Liu R.; Kao K.C. *J. Chem. Soc., Dalton, Trans*., **1998**, 1857–1862; (c) Lai C.K.; Len, Y.F. *Liq. Cryst.*, **1998**, *25*, 689–698; (d) Lai C.K.; Lu, M.Y.; Lin, F.J. *Liq. Cryst.* **1997**, *23*, 313–315.
(29) Kadkin, O.; Galyametdinov, Y.G.; Rakhmatullin, A. *Mol. Cryst. Liq. Cryst. Sci. Techol., Sect. A* **1999**, *332*, 109–118.
(30) Kadkin, O.; Galyametdinov, Y.G.;. Rakhmatullin A; Mavrin V.Y.; *Russ. Chem. Bull*. **1999**, *48*, 379–381.
(31) Ku, S.M.; Wu, Ch. Y.; Lai, C.K. *J. Chem. Soc., Dalton, Trans.* **2000**, 3491–3492.
(32) Binnemans, K.; Lodewyckx, K.; Donnio, B.; Guillon, D. *Chem. Eur. J.* **2002**, *8*, 1101–1105.
(33) Szydlowska, J.; Krowczynski, A.; Gorecka, E.; Pociecha, D. *Inorg. Chem*. **2000**, *39*, 4879–1885.
(34) Paschke, R.; Liebsch, S.; Tschierske, C.; Oakley, M.A.; Sinn, E.; *Inorg. Chem*. **2003**, *42*, 8230–8240.
(35) Barbera, J.; Gimenez R.; Marcos, M.; Serrano, J.L.; Alonso, P.J.; Martınez, J.I. *Chem. Mater*. **2003**, *15*, 958–964.
(36) Benouazzanne, M.; Coco, S.; Espinet, P. *Inorg. Chem.* **2002**, *41*, 5754–5759.
(37) Espinet, P.; Etxebarria, J.; Marcos, M.; Perez-Jubindo, M.A.; Ros, M.B.; Serrano, J.L. *Mater. Res. Soc. Symp. Proc.* **1995**, *392*, 123–133.
(38) Ghedini, M.; Pucci, D.; Crispini, A.; Aiello, I.; Barigelletti, F.; Gessi, A.; Francescangeli, O. *Appl. Organomet. Chem.* **1999**, *13*, 565–581.
(39) Lydon, D.P.; Cave, G.W.V.; Rourke, J.P. *J. Mater. Chem.* **1997**, *7*, 403–406.
(40) Neumann, B.; Hegmann, T.; Wolf, R.; Tschierske, C. *Chem. Commun.* **1998**, 105–106.
(41) (a) Lai, C.K.; Lin, R.; Lu, M.Y.; Kao, K.C. *J. Chem. Soc.* **1998**, 1857–1862; (b) Lai, C.K.; Leu, Y.F. *Liq. Cryst.* **1998**, *25*, 689–698.
(42) Zyss, J., Ed. *Molecular Nonlinear Optics: Materials, Physics and Devices*; Academic Press: Boston, MA, 1993.
(43) Bella, S.D.; Fragala, I.; Ledoux, I.; Marks, T.J. *J. Am. Chem. Soc*. **1995**, *117*, 9481–9485.
(44) Averseng, F.; Lacroix, P.G.; Malfant, I.; Perisse, N.; Lepetit, C.; *Inorg. Chem.* **2001**, *40*, 3797–3804.
(45) Sinn, E.; *Inorg. Chem*. **1976**, *15*, 358–365; 366–369; 2698–2712.
(46) Butcher, R.J.; Sinn, E. *Inorg. Chem.* **1976**, *15*, 1604–1608.
(47) Alapati, P.R.; Potukuchi, D.M.; Rao, N.V.S.; Pisipati, V.G.K.M. *Liq. Cryst.* **1988**, *3*, 1461–1480.
(48) Marcos, M.; Omenat, A.; Barbera, J.; Duran, F.; Serrano, J.L. *J. Mater. Chem.* **2004**, *14*, 3321–3327.
(49) Barbera, J.; Marcos, M.; Omenat, A.; Serrano, J.L.; Martinez, J.I.; Alonso, P.L. *Liq. Cryst*. **2000**, *27*, 255–262.
(50) Ghedini, M.; Armentano, S.; Bartolino, R.; Torquati, G.; Rustichelli, F. *Sol. State Comm.* **1987**, *64*, 1191–1194.

(51) Levelut, A.M.; Ghedini, M.; Bartolino, R.; Nicoletta, F.P.; Rustichelli F. *J. Physique* **1989**, *50*, 113–119.
(52) Torquati, G.; Francescangeli, O.; Ghedini M.; Armentano, S.; Nicoletta, F.P.; Bartolino, R. *Il Nuovo Cimento* **1990**, *12D*, 1363–1376.
(53) Albertini, G.; Guido, A.; Mancini, G.; Stizza, S.; Ghedini, M.; Bartolino, R.; *Europhys. Lett.* **1990**, *12*, 629–630.
(54) Goodby, J.W.; Gray G.W. In *Handbook of Liquid Crystals*; Vol. 1, Wiley-VCH: Weinheim, 1998.
(55) Marcos, M.; Romero, P.; Serrano, J.L.; Bueno, C.; Cabeza, J.A.; Oro, L.A. *Mol. Cryst. Liq. Cryst.* **1989**, *167*, 123–134.
(56) Ghedini, M.; Armentano, S.; Neve, F.; Licoccia, S. *J. Chem. Soc., Dalton Trans.* **1988**, 1565–1567.
(57) Szydlowska, J.; Krowczynski, A.; Gorecka, E.; Pociecha, D. *Inorg. Chem.* **2000**, *39*, 4879.
(58) Terazzi, E.; Benech, J.; Rivera, J.; Bernardinelli, G.; Donnio, B.; Guillon, D.; Piguet, C. *J. Chem. Soc., Dalton Trans.* **2003**, 769–772.
(59) Patel, D.B.; Bhattacharya, P.K. *Mol. Cryst. Liq. Cryst.* **2005**, *432*, 47–57.
(60) Keller, P.; Leibert, L. *Solid State Phys.* **1986**, *Supp. 14*, 19.
(61) Lai, C.K.; Leu, Y. *Liq. Cryst*. **1998**, *25*, 689–698.